HHS Public Access

Author manuscript

Neurobiol Dis. Author manuscript; available in PMC 2022 September 01.

Published in final edited form as:

Neurobiol Dis. 2022 September ; 171: 105801. doi:10.1016/j.nbd.2022.105801.

Somatostatin interneurons exhibit enhanced functional output and resilience to axotomy after mild traumatic brain injury

Alan C. Harris,

Xiao-Tao Jin[1],

John E. Greer,

John T. Povlishock,

Kimberle M. Jacobs[*]

Department of Anatomy & Neurobiology, Virginia Commonwealth University, Richmond, VA 23298, United States of America

Abstract

Mild traumatic brain injury (mTBI) gives rise to a remarkable breadth of pathobiological consequences, principal among which are traumatic axonal injury and perturbation of the functional integrity of neuronal networks that may arise secondary to the elimination of the presynaptic contribution of axotomized neurons. Because there exists a vast diversity of neocortical neuron subtypes, it is imperative to elucidate the relative vulnerability to axotomy among different subtypes. Toward this end, we exploited SOM-IRES-Cre mice to investigate the consequences of the central fluid percussion model of mTBI on the microanatomical integrity and the functional efficacy of the somatostatin (SOM) interneuron population, one of the principal subtypes of neocortical interneuron. We found that the SOM population is resilient to axotomy, representing only 10% of the global burden of inhibitory interneuron axotomy, a result congruous with past work demonstrating that parvalbumin (PV) interneurons bear most of the burden of interneuron axotomy. However, the intact structure of SOM interneurons after injury did not translate to normal cellular function. One day after mTBI, the SOM population is more

[*]Corresponding author: Kimberle.Jacobs@vcuhealth.org (K.M. Jacobs).

[1]Current affiliation for Xiaotao Jiang: Department of Physiology and Pharmacology, Wake Forest University, Winston-Salem, NC.

Author contributions

AH: data collection, data analysis, manuscript writing and revisions; XJ: data collection, data analysis, manuscript revisions; JG: data collection, data analysis, manuscript revisions; JP: study design, data collection, manuscript revisions; KMJ: study design, data collection, data analysis, manuscript writing and revisions.

All authors have approved the final version of the manuscript and agree to be accountable for all aspects of the work in ensuring that questions related to the accuracy or integrity of any part of the work are appropriately investigated and resolved. All persons designated as authors qualify for authorship, and all those who qualify for authorship are listed.

This work was supported by the National Institutes of HealthR01 NS077675.

CRediT authorship contribution statement

Alan C. Harris: Investigation, Formal analysis, Writing – original draft, Visualization. **Xiao-Tao Jin:** Investigation, Formal analysis. **John E. Greer:** Conceptualization, Methodology, Investigation, Formal analysis, Writing – review & editing, Visualization. **John T. Povlishock:** Conceptualization, Methodology, Writing – review & editing, Supervision, Funding acquisition. **Kimberle M. Jacobs:** Conceptualization, Methodology, Software, Formal analysis, Investigation, Writing – review & editing, Visualization, Supervision, Project administration, Funding acquisition.

Declaration of Competing Interest

None.

intrinsically excitable and demonstrates enhanced synaptic efficacy upon post-synaptic layer 5 pyramidal neurons as measured by optogenetics, yet the global evoked inhibitory tone within layer 5 is stable. Simultaneously, there exists a significant increase in the frequency of miniature inhibitory post-synaptic currents within layer 5 pyramidal neurons. These results are consistent with a scheme in which 1 day after mTBI, SOM interneurons are stimulated to compensate for the release from inhibition of layer 5 pyramidal neurons secondary to the disproportionate axotomy of PV interneurons. The enhancement of SOM interneuron intrinsic excitability and synaptic efficacy may represent the initial phase of a dynamic process of attempted autoregulation of neocortical network homeostasis secondary to mTBI.

Keywords

Inhibitory interneuron subtypes; Traumatic brain injury; Axonal injury; Cortical network; Optogenetics

1. Introduction

Mild traumatic brain injury (mTBI) is a ubiquitous public health scourge within the United States. While the annual incidence of documented cases of mTBI numbers around 300 per 100,000 people, a marked fraction of those who sustain mTBI seek private medical care or do not seek medical care at all; therefore, the true annual incidence of mTBI has been estimated at 500–600 per 100,000 people (Bazarian et al., 2005). While the majority of patients who sustain mTBI recover to their pre-injury neurological baseline within three months subsequent to injury, a minority—15–30%—of patients experience chronic deficits within various cognitive and mood-related domains (Babcock et al., 2013; McMahon et al., 2014). Patients belonging to this minority commonly report disruption in the ability to concentrate and to manipulate working memories toward the execution of complex tasks. In order to develop effective therapeutics toward the alleviation of the mental disruption encountered by this group, the underlying pathophysiology of trauma-induced cognitive changes must be elucidated.

A pathognomonic sequela of mTBI is traumatic axonal injury (TAI), the burden of which correlates with less favorable functional outcomes (van Eijck et al., 2018; Yuh et al., 2013). TAI is concentrated in vulnerable anatomical foci and emerges secondary to traumatic shear- and tensile-force induced disruption of the dynamics of the intra-axonal cytoskeletal network. The focal disruption of the intra-axonal cytoskeleton congests anterograde transport and gives rise to areas of progressive accumulation of organelles and axonal cargo (Povlishock et al.,1983; Povlishock and Christman, 1995; Smith et al., 2013). Distal to this site, the axon ultimately disconnects, and the subsequent degeneration and deafferentation of the distal axon may give rise to derangement of the flow of information within neocortical networks and associated cognitive dysfunction. While seminal investigations of the pathobiology of mTBI focused on TAI within subcortical white matter tracts (Adams et al., 1991; Blumbergs et al., 1994; Kinnunen et al., 2011), TAI emerges within neocortical gray matter as well (Greer et al., 2013; Greer et al., 2012). Because subcortical and

neocortical TAI respond differentially to attempted neuroprotective interventions (Hånell et al., 2015b), divergent mechanisms may govern the emergence of TAI within each region.

Recent work has begun to investigate the extent to which the burden of gray matter TAI is borne by the population of neocortical GABAergic inhibitory interneurons (Vascak et al., 2018). Within the neocortex, inhibitory interneurons substantially amplify the capacity for information synthesis of ensembles of excitatory pyramidal neurons (PNs) (Hu et al., 2014). By means of ultra-precise modulation of excitatory input to PNs via mechanisms like feedforward and feedback inhibition, in conjunction with targeted synaptic control of specific microanatomical domains of PNs, inhibitory interneurons sculpt complex temporal dynamics into the flow of information within neuronal networks (Jonas et al., 2004; Pouille and Scanziani, 2001). Therefore, it is imperative to elucidate the extent to which the population of neocortical interneurons is susceptible to TAI, as damage to this population might give rise to profound derangement of neocortical function. Toward this end, Vascak et al. (Vascak et al., 2018) used PV-Cre;Ai9-tdTomato mice to demonstrate that mTBI gives rise to perisomatic axonal injury within approximately 10% of the population of PV interneurons throughout neocortical layers 2–6. Furthermore, having validated GAD67+ swellings as a signature of axotomy specific to inhibitory interneurons, it was found that of all GAD67+/APP+ perisomatic axonal swellings within the neocortex, 98% of this group was GAD67+/APP+/tdTomato+. This result suggested that PV interneurons are especially vulnerable to traumatic axotomy and represent nearly the entire set of inhibitory interneurons sensitive to traumatic axotomy.

The diversity of interneurons is vast and indefinite (DeFelipe et al., 2013; Gouwens et al., 2020; Jiang et al., 2015; Markram et al., 2004); however, it is broadly accepted that three principal classes are dissociable on the basis of expression of the neuropeptide somatostatin (SOM), the calcium-binding protein PV, or the 5HT-3a ligand-gated ion channel (Rudy et al., 2011). SOM interneurons put forth synapses biased for the distal dendrites of PNs and distribute dense inhibition within neocortical networks. It has been posited that SOM interneurons distribute inhibition indiscriminately to the PNs within the range of their axonal arbor (Fino and Yuste, 2011), although targeted inhibition of specific PN subtypes within layer 5 has been demonstrated (Hilscher et al., 2017). Owing to this blanket inhibition and to the facilitating nature of PN-to-SOM synapses, SOM interneurons mediate a process of frequency-dependent di-synaptic inhibition (Silberberg and Markram, 2007), in which active PNs inhibit as a function of their degree of activation the PNs in their vicinity. Thus SOM interneurons sharpen the contrast of afferent information streams and appear to play a role in the generation of rhythmic activity (Antonoudiou et al., 2020; Hakim et al., 2018; Veit et al., 2017).

In order to probe for the existence of differential susceptibility to trauma among the principal subclasses of interneurons, the present study made use of SOM-IRES-Cre driver mice to label SOM interneurons selectively and investigate the effects of trauma on this subclass. SOM-IRES-Cre driver mice were mated with tDTomato mice to investigate the consequences of trauma on the axonal integrity of SOM interneurons, or with ChR2-EYFP mice to probe for trauma-induced alterations of SOM synaptic efficacy at post-synaptic layer 5 PNs. We found that although axotomy within the SOM population was rare, nonetheless

SOM interneurons are more intrinsically excitable and exert a potentiated synaptic efficacy at PNs secondary to mTBI. Comprehensive electrophysiological experiments suggest this amplification of SOM synaptic efficacy may arise as a function of an increase in the density of SOM-to-PN synapses. The enhancement of SOM synaptic efficacy may arise as a compensatory response to traumatic PV interneuron deafferentation and thus function to restore the network toward a target range of the relative strength of inhibition and excitation.

2. Methods

All methods conform to the institutional animal care and use committee regulations of Virginia Commonwealth University, protocols AD20102 and AD10001868. A total of 52 male mice were used throughout the course of the present study (physiology in ex vivo slices: $N = 43$ mice consisting of 28 control and 15 mTBI; immunohistochemistry: $N = 9$ mice, consisting of 2 control and 7 mTBI). To exploit optogenetics to measure the synaptic efficacy of SOM interneurons, SOM-IRES-Cre mice (Jackson Labs, stock #013044) were bred with Ai32 (RCL-ChR2(H134R)/EYFP) mice (Jackson Labs, stock #012569), thus generating offspring that expressed the light-gated ion channel ChR2 selectively in SOM interneurons. To label SOM interneurons selectively for immunohistochemical studies of axonal injury, SOM-IRES-Cre mice were bred with Ai9(RCL-tdT) mice (Jackson Labs, stock #007909), thus producing tdTomato in SOM interneurons. To model mTBI with TAI, mice received a central fluid percussion injury (cFPI), which reproduces many of the salient features of the pathobiological sequelae of mTBI in humans. Of particular importance, the cFPI model gives rise to TAI with the magnitude of injury under precise experimental control, and without giving rise to confounding sequelae such as gross parenchymal lesions, neocortical contusion or neuronal death (Greer et al., 2011; Shultz et al., 2017). In both mTBI and sham groups, mice underwent a midline craniectomy procedure, in which a 3-mm diameter disc of the calvarium was excised to expose the intact dura. This operation typically took approximately one hour. Around this site, an injury hub was affixed by cyanoacrylate and secured by dental cement. After a one-hour period of recovery, mice of the cFPI group were administered 4% isoflurane for 4 min, the injury hub was filled with sterile saline, and the mice were securely attached to a custom-fabricated cFPI device. By means of a weighted pendulum striking a fluid-filled tube, this device directed a short-impulse (~15 msec) wave of pressure onto the intact dura, thus modeling the type of acceleration-deceleration injury characteristic of common closed-head injuries in humans. Sham mice were treated in an equivalent manner, except that the pendulum was not released. Subsequent to injury or sham, mice were removed from the device and monitored for spontaneous return of the righting reflex. Finally, the hub was removed and the site of incision sutured. Time required for spontaneous return of the righting reflex after trauma—a correlate of the duration of loss of consciousness in humans—was consistently within the range of 5–8 min. Mice were returned to a warmed holding cage and monitored for signs of distress before being returned to the vivarium prior to further experimentation.

For quantitative assessment of somatostatin axotomy, at 3 h survival mice received a lethal dose of sodium pentobarbital. After loss of pain reflexes, mice were transcardially perfused with 4% paraformaldehyde for 10–20 min. Brains were dissected and immersed in 4% paraformaldehyde overnight at 4 °C. Brains were then sectioned coronally at 40 μm using

a vibratome (Leica VT1000S). For quantitative studies, 3 sections randomly selected from section 1.5–2.5 mm posterior to bregma were chosen due to previous work demonstrating a significant burden of TAI in the glutamatergic pyramidal neurons and PV interneurons within the primary somatosensory cortex (S1).

Free-floating sections were rinsed with PBS and then incubated for 1 h at room temperature with 10% normal goat serum and 0.5% Triton X-100 in PBS. To mask any potential endogenous mouse immunoglobulin, the blocking buffer was supplemented with Mouse-on-Mouse reagent (MOM; Vector Laboratories, MKB-2213). Then sections were rinsed with 1% normal goat serum, and 0.5% Triton X-100 in PBS (working buffer). Primary antibody solutions were prepared by dilution with working buffer, and the sections were incubated overnight at 4 °C. Specifically, we used antibodies against RFP (rabbit, 1:1000, 600-401-379; Rock-land) and GAD67 (mouse IgG2a, clone 1G10.2, 1:1000; Millipore, MAB5406). As previously reported, anti-RFP antibodies were utilized to amplify and stabilize signals from the SOM-driven tdTomato fluorophore (Vascak et al., 2018). The following day, sections were rinsed with working buffer and incubated with appropriate goat-derived secondary antibodies conjugated to Alexa Fluor 488 and 594 (1:500: Thermo Fisher Scientific) for 2 h at room temperature. After final rinses using working buffer then PBS, sections were mounted on glass slides and cover-slipped using non-hardening Vectashield ± DAPI (Vector Laboratories, H-1000 or H-1200).

Sections were imaged at 20× by means of a Keyence BZ-X800 fluorescent microscope, and GAD67 immunopositive swellings were identified and counted manually throughout the somatosensory neocortex bilaterally. An area 2 mm lateral to midline (to exclude motor cortex) and extending to the lateral extent of the hippocampus demarcated the region of interest. GAD-67 positive swellings were identified and quantified throughout all layers of the neocortex, and assessed for colocalization with RFP/tdTomato, indicating SOM expression. Tiled 4× montage images were captured to measure total area of the ROI for each section. A Student's *t*-test was utilized to compare the mean number of SOM+ swellings between the injured and sham-injured groups.

For physiological experiments, 1 day after injury induction, the behavior of the mice of each group was assessed. Mice of the mTBI group did not display gross behavioral derangement or signs of distress. Subsequently, mice were deeply anesthetized with isoflurane and rapidly perfused through the aorta with ice-cold, sucrose-substituted artificial cerebrospinal fluid (aCSF) previously saturated with a mixture of 95% O_2 / 5% CO_2. This aCSF contained (in mM): 234.0 sucrose, 2.5 KCl, 1.25 NaH_2PO_4 • H_2O, 10.0 $MgSO_4$ • H_2O, 0.5 $CaCl_2$ • $2H_20$, 26.0 $NaHCO_3$, 11.0 glucose. The brain was extracted and chilled in a beaker of this sucrose-substituted aCSF before 300 μm-thick slices containing somatosensory cortex were prepared by a Leica VT 1200S vibratome. These sections were bisected at the midline and gently transferred to a holding chamber containing a physiological aCSF held at 34 °C and bubbled with a mixture of 95% O_2 / 5% CO_2. This aCSF contained (in mM): 126.0 NaCl, 3.0 KCl, 1.25 NaH_2PO_4 • H_2O, 2.0 $MgCl_2$ • $6H_2O$, 2.0 $CaCl_2$ • $2H_2O$, 10.0 glucose. Slices were maintained at 34 °C for 25 min, after which they were allowed to acclimate to room temperature (at least an additional 20 min). All electrophysiological experiments were

conducted in a recording aCSF containing (in mM): 126 NaCl, 3.5 KCl, 1.25 NaH_2PO_4 • H_2O, 1.0 $MgSO_4$ • $7H_2O$, 1.2 CaCl • $2H_2O$, 10 glucose.

In order to conduct single-cell optogenetic experiments, slices thus prepared were transferred to an immersion-style chamber under constant perfusion (2–3 mL / minute) by a physiological aCSF maintained at 30° C. Pyramidal neurons of layer 5 of the somatosensory cortex were identified under Dodt gradient contrast microscopy (Zeiss AxioExaminer) by the shape of the somata and the presence of a thick apical dendrite. For experiments involving SOM interneurons, cells were targeted on the basis of their EYFP fluorescence. Patch electrodes were pulled from borosilicate glass capillaries using a vertical puller (Narishige, model PC-10) to a final resistance of 3–5 MΩ. Seals of >1 GΩ resistance were formed onto targeted neurons, and capacitative transients were compensated prior to breaking in and initiation of whole-cell mode. Data were acquired using a Multiclamp 700B amplifier and digitized at 200 Hz by a Digidata 1440A running pClamp software (both Molecular Devices, San Jose, CA). The intracellular solution was a high-chloride formulation containing (in mM): 70 KCl, 70 K-gluconate, 10 HEPES, 4 EGTA, 4 Na-ATP, 0.2 Na-GTP, and 0.4% biocytin. This solution was chosen to render GABA-A-mediated currents depolarizing, thus allowing the measurement of inhibitory currents and assessment of action potential (AP) firing properties within a single neuron. Spontaneous and optogenetically- or electrically-evoked inhibitory postsynaptic currents (s-, o-, e- IPSCs) were measured at a holding potential of −70 mV in the presence of the glutamate receptor antagonists APV (50 μM) and DNQX (20 μM). Miniature inhibitory postsynaptic currents (mIPSCs) were measured in the additional presence of tetrodotoxin (1 μM). The sIPSCs were recorded prior to the initiation of optogenetic or electrical stimulation experiments, while mIPSCs were recorded either as the terminal experiment or within separate slices.

For optogenetic experiments, blue LED-generated light was emitted onto the field within the vicinity of the recorded neuron through a 60× water-immersion objective positioned over the recorded neuron. The duration of light emission was systematically increased (2, 10, 20, 30 and 40 msec) to establish an intensity series, and the resulting optogenetically-evoked, SOM interneuron-mediated IPSCs were recorded. For repetitive stimulation experiments, five consecutive 2 msec pulses of blue light were shone at 40 Hz. To record the IPSC contributed by the total population of local inhibitory interneurons, a stimulating electrode was pulled from borosilicate glass, filled with 1 M NaCl solution, and situated 100–200 μm lateral to the recorded neuron. A stimulus isolator unit (World Precision Instruments, model A362) was used to identify the threshold of electrical stimulation, defined as the current amount that gave rise to an electrical IPSC in approximately 50% of trials. This threshold value was systematically doubled up to 16× in order to establish an electrical intensity series. Finally, to probe for trauma-induced alterations in SOM interneuron synaptic efficacy over the total population of inhibitory interneurons, the objective was repositioned over the stimulating electrode. Blue light was shone simultaneously with the electrical stimulation and for 70 msec afterward, and the resulting electrical + light IPSC was measured. Finally, cellular identity was confirmed in current clamp mode by injection of square waves of depolarizing current and assessment of the kinetics and phenotype of the resulting trains of action potentials.

For experiments assessing the SOM-to-SOM synaptic efficacy and the intrinsic properties of SOM interneurons, $EYFP^+$ cells were identified under fluorescence and subsequently targeted for patch clamp recordings under DIC illumination. Optogenetic and current clamp experiments were conducted in an equivalent manner to those within pyramidal neurons. SOM interneurons were held at −65 mV for current clamp experiments.

2.1 Statistical analyses

For this study we are comparing our sham-injured controls to the mild cFPI model of TBI. Thus in cases of single measures, the Students, *t*-test was utilized and calculated within Microsoft Excel. In all cases the individual was considered to be the recorded neuron. A number of measures had intensity series or repeated stimulation which are both effectively repeated measures, and thus in these cases a repeated measures 2-way ANOVA was performed in SPSS software (IBM). In all cases significance was considered $p < 0.05$ and the statistical test used is listed in each figure legend.

3. Results

Our group has demonstrated previously that of all trauma-induced $GAD67^+/APP^+$ perisomatic axonal swellings within neocortex, >90% are borne by PV interneurons (Vascak et al., 2018). This result suggested that PV interneurons are highly vulnerable to traumatic axotomy and represent nearly the entire cohort of the axotomized inhibitory interneurons. Accordingly, we hypothesized that the subclass of somatostatin (SOM) interneurons would be resilient to traumatic forces and remain structurally intact after mTBI. To measure the burden of axotomy borne by the SOM interneuron population, we subjected male SOM-Cre;Ai9-tDTomato mice to mTBI and probed for co-localization of tDTomato with $GAD67^+$ retraction bulbs, which are a pathobiological signature of interneuron axotomy. Similar to previous strategies for studying interneuron axotomy, the use of genetically driven fluorescent proteins enabled detection of rare and subtle axonal pathology following mTBI in the SOM population. Although detected (Fig. 1E) following cFPI, axotomy within the SOM population was rare, representing only 10% of the axotomy occurring in GAD67+ swellings within the somatosensory cortex (Fig. 1H), and minute axonal swellings were detectable along the length of the SOM axon (Fig. 1F–G).

The previous discovery that structurally intact layer 5 pyramidal neurons nevertheless manifest trauma-induced derangement of intrinsic membrane properties (Greer et al., 2012) spurred the investigation here of the intrinsic membrane properties of SOM interneurons subsequent to trauma. Floxed ChR2-EYFP mice were crossed with SOM-IRES-Cre mice, and fluorescent interneurons were targeted for whole-cell patch clamp recordings. Most SOM interneurons of both control and mTBI groups displayed the classical electrophysiological phenotype ascribed to this class, which is characterized by a marked I_h-mediated sag current, action potentials elicited upon cessation of hyperpolarizing current injection, adaptation, and an initial afterhyperpolarization that is more hyperpolarized than terminal afterhyperpolarizations in the train (Fig. 2A–D). There were no differences between mTBI and sham conditions on metrics of input resistance, action potential (AP) threshold, or rheobase (Table 1). After trauma, the SOM interneurons did have a significantly more

depolarized resting membrane potential (Fig. 2E). However, there was no association between the difference in resting membrane potential and the likelihood of encountering spontaneous firing, a characteristic behavior of SOM interneurons recorded under conditions of elevated extracellular potassium (Urban-Ciecko et al., 2015). The time from the onset of the depolarizing current injection to the first AP at rheobase was significantly shorter for the mTBI group (Fig. 2F), and the slope of the plot of AP frequency versus injected current was significantly larger in the mTBI group (Fig. 2G). Taken together, these results suggest that independent of axotomy, there is a trauma-induced enhancement of intrinsic excitability within the SOM interneuron population. Finally, the degree of adaptation, defined as the frequency of the first AP pair divided by the frequency of the last AP pair for sweeps with 8–10 APs, was increased in SOM interneurons within the mTBI group. Thus, for a given level of current injection, SOM interneurons within the trauma condition fire more APs which emerge earlier and at a higher frequency and which subsequently decelerate to a greater degree compared to the sham condition.

Prior to initiation of current clamp experiments to assess the intrinsic membrane properties of SOM interneurons, the successful targeting of each cell was verified by the presence of a blue LED-induced excitatory current. Under recording conditions in which inhibitory currents were rendered depolarizing, most $ChR2^+$ cells in each condition manifested a biphasic waveform in response to stimulation of the field by blue LED. It was expected that the initial peak, which occurred within 1 msec, represented direct ChR2-mediated activation, while the delayed, subsequent peak represented activation of SOM-to-SOM synapses and/or autapses. Although connections between SOM interneurons have in some cases been reported to be low (Gibson et al., 1999), other reports have also found chemical synaptic contacts between SOM interneurons (Fino and Yuste, 2011). Consistent with this notion, 10 μM gabazine applied within the bath abolished the second peak but not the first peak of the biphasic waveform (Fig. 3A). There was no difference in the amplitudes of either the first or second peaks recorded in injured compared to sham control cortex, although there existed markedly greater variability within the amplitude of the second peak (synaptic portion of the waveform) within the mTBI condition (Fig. 3C).

Given that PV interneurons put forth chemical synapses onto SOM interneurons (Gibson et al., 1999; but also see Pfeffer et al., 2013) and that we have previously shown that PV interneurons are axotomized after injury (Vascak et al., 2018), it was expected that the previously demonstrated PV axotomy might give rise to a reduction of the frequency of spontaneous inhibitory post-synaptic currents (sIPSCS) recorded in SOM interneurons. While no significant difference in the frequency or amplitude of sIPSCs recorded in SOM interneurons was detected, there was a significant slowing of the mean weighted decay tau in the mTBI condition compared to controls (Fig. 4). This slowing could arise secondary to an increase in relative dominance of dendritic versus somatic inhibition.

In addition to the selective vulnerability of PV interneurons to axotomy, our group has previously detected a significant reduction of the density of PV^+ synapses onto the perisomatic region of pyramidal neurons subsequent to mTBI (Vascak et al., 2017). Because SOM interneurons remain intact after trauma, we hypothesized that SOM interneurons might fill in the synaptic territory relinquished by damaged PV interneurons, as axonal

sprouting has been demonstrated to occur within 1 day of mTBI. Such an increase of SOM interneuron synaptic density would be expected to manifest at the functional level as an enhancement of SOM-mediated IPSCs. In order to probe for trauma-induced, network-scale alterations in the efficacy of SOM interneurons, patch clamp recordings were made from layer 5 pyramidal neurons within ChR2-EYFP;SOM-IRES-Cre mice while activating the SOM interneurons in the vicinity by blue LED applied through a 60× objective positioned over the recorded neuron. In order to rule out any trauma-induced alteration of the function of ChR2 itself, we first recorded from ChR2-expressing SOM interneurons and measured the number of action potentials elicited by various durations of blue light. ChR2 behaved similarly in SOM interneurons of the mTBI and sham conditions (Fig. 5A–B), and there was no significant difference in the relation of the duration of light to the number of APs elicited (Fig. 5C). Activation of the field of SOM interneurons gave rise to an inhibitory postsynaptic potential within pyramidal neurons (Fig. 5E). Strikingly, activation of the field of SOM interneurons during a train of APs elicited in a pyramidal neuron by current injection could abort an intra-train AP (Fig. 5D). Given that this means of activating SOM was equally effective in control and mTBI conditions, the synaptic efficacy of the SOM connection to pyramidal neurons could be measured via the light-evoked IPSC recorded in pyramidal neurons. Recordings of the light-induced IPSC within pyramidal neurons showed a significant increase in the amplitude for the mTBI condition compared to controls (Fig. 6A–C). There was no difference between the duration of the light-induced IPSC between mTBI and controls (Fig. 6D).

This amplification of the light-induced IPSC after mTBI may arise by a presynaptic mechanism, either as a consequence of an increase in the quantity and/or density of SOM-to-PN synapses, or an increase in the probability of the release of vesicles from an equivalent quantity of SOM-to-PN synapses, or as a combination of these two. To distinguish between these alternatives, we conducted experiments to assess any trauma-induced change in the probability of release. Specifically, the field of SOM interneurons was repetitively activated with light at 20 Hz, and the degree of depression obtained in the consequent series of IPSCs within post-synaptic PNs was recorded. The peak amplitudes of light-evoked IPSCs were significantly greater for each stimulation within the mTBI condition compared to sham (Fig. 7C). There was no significant difference in the relative depression within the series of repetitive IPSCs (Fig. 7D), thus suggesting that mTBI did not alter release probability.

These results suggested that if the increased output was due to an increased quantity of SOM-to-PN synaptic terminals, we would detect a corresponding increase in the frequency of sIPSCs recorded from PNs, although a simultaneous decrease in the quantity of PV-to-PN synapses may mask this effect. There was a significant increase in both sIPSC and mIPSC events recorded in layer 5 PNs of the mTBI group compared to controls (Fig. 8). The amplitudes of both s- and m-IPSCs were unaltered after mTBI compared to controls.

Our results support the premise that mTBI causes two competing functional effects on the total interneuron population, in which axotomy of ~10% of the PV population leads to a reduction of PV-to-PN synaptic efficacy and concomitant enhancement of SOM-to-PN synaptic efficacy, possibly as a compensatory response. To examine whether the increased output from SOM interneurons compensated for the loss of PV inhibition at

the network level, the field 100–200 μm lateral to a recorded pyramidal neuron was electrically stimulated under conditions of total ionotropic glutamate receptor blockade. This monosynaptic eIPSC recorded from layer 5 PNs was similar in amplitude and duration at all stimulus intensities for control compared to mTBI neurons (Fig. 9). Thus, in PNs when measuring the overall inhibition that can be evoked electrically, the loss of PV-mediated inhibition may be compensated by the increase in SOM-mediated inhibition.

Because SOM interneurons synapse onto PV interneurons as well as PNs (Cardin, 2018; Gibson et al., 1999; Pfeffer et al., 2013; Yavorska and Wehr, 2016), we reasoned that stimulating the field of SOM interneurons with light *simultaneous* to the electrical stimulation of the total interneuron population would allow measurement of the efficacy of this SOM-to-PV connection and evaluation of its relation to trauma. Therefore, in a subset of pyramidal neurons, subsequent to recording the eIPSC, with the objective positioned over the site of electrical stimulation, a pulse of blue light was applied simultaneously with the electrical stimulation, lasting 70 msec after the electrical stimulation. This addition of light activation of SOM interneurons had minimal effect in control slices (Fig. 10A, C, E). In contrast, light activation of SOM interneurons significantly decreased the amplitude of the eIPSC within the mTBI group (Fig. 10B, D, F), suggesting a strengthening of SOM-mediated inhibition onto PV interneurons. When calculated as percent change (the electrical plus light response divided by the electrical only response), for control slices this value was near 100%. In contrast, for the mTBI group this value was reduced by nearly 50% (Fig. 10H).

4. Discussion

The results of the present study indicate that SOM interneurons are not merely resilient to trauma, but may assume an enhanced functional influence within the neocortical network during the immediate phase after concussive head trauma. We posit that this enhancement of SOM interneuron functional influence may represent a compensatory response to the loss of inhibition induced by traumatic axotomy of PV interneurons. Because SOM and PV interneurons have divergent morphologies, zones of projection, afferent connections and functional specializations within neocortical networks, the emergence of distorted functional efficacy between these cardinal interneuron subtypes may substantially modify the global dynamics of the neocortical network, at least during the immediate post-traumatic interval.

It has been appreciated for some time that moderate to severe TBI induced with either lateral fluid percussion injury or controlled cortical impact (CCI) models can induce a loss of inhibitory interneurons as assessed by immunohistochemistry as well as a reduction of functional inhibition (Lowenstein et al., 1992; Santhakumar et al., 2000; Santhakumar et al., 2001; Toth et al., 1997). Within the hippocampus, hilar interneurons are particularly affected (Folweiler et al., 2020; Frankowski et al., 2019; Gupta et al., 2012; Hunt et al., 2011; Lowenstein et al., 1992). Neocortical inhibition is also reduced within models of moderate to severe injury that feature partial deafferentation (Avramescu et al., 2009; Cantu et al., 2015; Carron et al., 2020; Frankowski et al., 2021; Hameed et al., 2019; Hsieh et al., 2017; MacMullin et al., 2020; Nichols et al., 2018). In most of these cases, as well as with the milder weight drop model of injury, a loss of inhibitory interneurons has been

demonstrated (Carron et al., 2016; Carron et al., 2018; but see Gu et al., 2017). We note that in our mild cFPI model, there is no loss in the quantity of GABAergic interneurons in the cortex (Vascak et al., 2018). PV interneurons have been shown to be particularly vulnerable to head trauma both in the hippocampus (Folweiler et al., 2020; Frankowski et al., 2019; Griffiths et al., 2019; Huusko et al., 2015; Santhakumar et al., 2000; Toth et al., 1997; Tucker et al., 2019; Zhang et al., 2018) and in the cortex (Cantu et al., 2015; Carron et al., 2020; Hameed et al., 2019; Hsieh et al., 2017; MacMullin et al., 2020; Nichols et al., 2018). Fewer studies have looked at SOM interneurons. Using lateral fluid percussion injury or CCI in adult models, a loss of SOM interneurons was found in both hippocampus and cortex (Cantu et al., 2015; Frankowski et al., 2019; Lowenstein et al., 1992). In contrast, in the mild weight drop model and in juvenile CCI, no change in the quantity of SOM interneurons was found (Carron et al., 2016; Nichols et al., 2018). In the Nichols study, PV interneurons were decreased at the same locations where SOM interneurons were unchanged. In the Carron study, there were no changes in the numbers of PV, SOM, NPY, or calbindin interneurons, but there was a decrease in the number of calretinin neurons in the superficial layers ventral to the injury site, in addition to differential effects on inhibitory interneuron subtypes within the hippocampus, yet no change in hippocampal SOM interneurons (Carron et al., 2016). Our studies represent the first to show differential effects on inhibitory interneuron subtype structure and function after TBI without the loss of interneurons. It is not surprising that more severe injuries affect multiple inhibitory interneuron subtypes. In contrast, within our mild cFPI model and within the juvenile CCI model, SOM interneurons are resilient, while PV interneurons are either lost or axotomized, reducing their functional efficacy (Nichols et al., 2018; Vascak et al., 2018). Interestingly, in temporal lobe epilepsy, SOM interneurons are lost while PV are more resilient (Sloviter, 1987; Sloviter, 1989; Sloviter et al., 1991). Differential vulnerability of interneuron subtypes has been demonstrated under other conditions affecting both developing and adult animals (Botterill et al., 2017; George and Jacobs, 2011; Kuruba et al., 2011; Marx et al., 2013; Pizzo et al., 2016). It is not clear why PV interneurons are axotomized while SOM interneurons remain intact after mild traumatic brain injury. However, perineuronal nets, which have been shown to be altered after TBI (Hsieh et al., 2017; MacMullin et al., 2020; Wiley et al., 2016) envelope the terminals of PV interneurons but not those of SOM interneurons (Celio et al., 1998; Wingert and Sorg, 2021).

PV interneurons put forth synapses biased for the somata and proximal dendrites of pyramidal neurons, and thus are anatomically positioned to exert potent inhibitory control of pyramidal neurons (Hu et al., 2014). PV-mediated inhibition is crucial for the emergence of gamma-frequency synchronization and the orderly routing of information in the time domain (Cardin et al., 2009; Fries et al., 2007; Sohal et al., 2009). Consequently, PV interneuron axotomy may selectively release pyramidal neurons from the dominant form of inhibition, thus disrupting the delicate excitatory-inhibitory balance within the network and catalyzing amplified network excitability (Hånell et al., 2015a). Neuronal networks tend to maintain a target range of activity in the face of perturbations by tuning neuronal membrane conductance properties and/or adjusting the synaptic efficacy of various cell types (Desai et al., 1999; Evans et al., 2015; Swanwick et al., 2006; Turrigiano and Nelson, 2004), and significant increases in neocortical inhibitory synaptic density have

been shown to emerge within 24 h in response to continuous whisker stimulation in mice (Knott et al., 2002). The data of the present study are consistent with a scheme in which after mTBI, SOM interneuron intrinsic membrane properties and synaptic efficacy self-adjust to compensate for the selective deafferentation of pyramidal neuron somata by axotomized PV interneurons, which previously has been demonstrated to arise after mTBI (Vascak et al., 2018). Specifically, the elevated F–I slope, depolarized resting membrane potential and accelerated adaptation of SOM interneurons suggest that SOM interneurons evolve into a more excitable state after mTBI. In addition to these alterations of SOM interneuron intrinsic membrane properties, optogenetic activation of SOM interneurons revealed a significantly enhanced amplitude of the SOM-mediated IPSC recorded at post-synaptic pyramidal neurons after mTBI. Because the percent relative depression produced by repetitive optical stimulation at 20 Hz was not significantly different between mTBI and sham, the increased output is unlikely to be attributable to an increase in the probability of release at SOM-to-PN terminals. Simultaneously, no difference was detected between the amplitudes of the IPSCs recorded at pyramidal neurons in response to electrical stimulation of the total population of inhibitory interneurons, suggesting any reduction of PV synaptic efficacy was approximately balanced by the enhancement of SOM synaptic efficacy. In conjunction with an increased frequency but not amplitude of both s- and mIPSCs, these data may indicate that the quantity and/or density of SOM-to-PN synapses expands after mTBI. Alternatively, an equivalent density of SOM interneuron synapses may migrate to a position more proximal to the pyramidal neuron soma. Because there exists no means to distinguish between these alternatives via electrophysiology, future experiments will assess the position of SOM interneuron synapses relative to the pyramidal neuron soma after mTBI, probing for the presence of a more proximal synaptic distribution.

Despite the lack of difference between mTBI and sham in the amplitude of the electrically-evoked IPSC contributed by the total population of interneurons, there existed a striking difference in the inhibitory efficacy of the SOM interneuron subpopulation over the total population of interneurons itself (Fig. 9). In other words, the addition of optogenetic stimulation of the SOM interneuron population significantly attenuated the amplitude of the electrically-evoked IPSC contributed by the total population of interneurons. The physical interpretation of this finding may be that after mTBI, SOM interneurons are stimulated to put forth synapses indiscriminately within the domain of their axonal arbor.This synaptic expansion may thus compensate for the PV-to-PN synapses relinquished by axotomized PV interneurons, yet simultaneously function antagonistically by enhancing inhibition onto intact PV interneurons and onto other SOM interneurons. Although SOM interneurons have been proposed not to inhibit other SOM interneurons (Pfeffer et al., 2013), we detected a $GABA_A$ receptor-dependent IPSC within SOM interneurons upon optogenetic stimulation of the SOM interneurons within the local field (Fig. 5). This result constitutes evidence of the existence of SOM-to-SOM synapses in most of the SOM cells recorded in this study. These SOM-to-SOM synapses may be contributed between SOM cells or could exist as autapses. The indiscriminate formation by SOM interneurons of post-synaptic contacts has been proposed to occur among pyramidal cells (Fino and Yuste, 2011). Thus, it is plausible that SOM interneurons may non-selectively target post-synaptic inhibitory interneurons. Such haphazard propagation of synapses by SOM interneurons may render the

attempted homeostatic response to trauma maladaptive, as skewed synaptic weights between interneuron types could give rise to derangement of rhythmogenesis and faulty routing of information by thalamocortical afferents. These synapses may subsequently be pruned, as it has been reported using the lateral fluid percussion injury model that IPSCs in layer 5 pyramidal neurons are significantly reduced compared to sham 7 days after mTBI (Shultz et al., 2017). Thus, the state of the network exhibited in the present study may represent an ephemeral phase of a dynamic process of attempted restoration of network homeostasis after mTBI.

How might the differential susceptibility to traumatic axotomy between PV and SOM interneurons affect the emergence of oscillatory phenomena, cognition and behavior? Gamma oscillations may represent a critical component of sensory perception, and thus their disruption may give rise to cognitive dysfunction. Recent experiments have suggested a relationship between the PV to SOM ratio and the power of gamma oscillations. If PV interneurons are disproportionately axotomized while SOM interneurons are spared, the ratio of inhibition mediated by PV:SOM interneurons is expected to decrease. Various methods of diminishing signaling through the receptor tyrosine kinase ErbB4 converge on reducing the inhibitory efficacy of PV interneurons while SOM interneurons are largely spared. Using such methods, one study reported a decrease in the power of gamma band oscillations within CA1 elicited by kainic acid (Kawata et al., 2017), while another study reported an increase in the power of spontaneous gamma band oscillations within CA1 in freely moving mice (Del Pino et al., 2013). In addition, heterozygotic knockout of the Dlx5/6 homeobox transcription factors selectively impaired the intrinsic membrane properties and synaptic efficacy of fast-spiking interneurons by 10 weeks of age, and these deficiencies were associated with increased power of prefrontal cortexregional spontaneous gamma band oscillations, decreased power of task-evoked gamma band oscillations, and increased perseverative errors in a behavioral task requiring rule-shifting (Cho et al., 2015). Conversely, conditional knockout of PTEN within the medial ganglionic eminence and pre-optic area gives rise to a reduction in the quantity of SOM interneurons and an increase in the quantity of PV interneurons, thus boosting the PV:SOM ratio. Enhancement of the PV:SOM ratio was associated with a decrease in the power of PFC-regional spontaneous gamma oscillations and an increase in the power of gamma oscillations evoked by social interaction (Vogt et al., 2015). Taken together, it is logical to hypothesize that the decrease in relative efficacy of PV:SOM interneurons that arises after mTBI may cause an enhancement in the power of spontaneous gamma oscillations and simultaneous reduction of task- or stimulus-evoked gamma oscillations. Future experiments will use in vivo electroencephalographic measurements to investigate the consequences of mTBI on the power of gamma oscillations associated with distinct brain states. In addition we note that these studies were conducted only on male mice, as were our previous relevant studies, including that identifying that it is primarily the PV subtype of interneuron that is axotomized after injury (Vascak et al., 2018). Evaluation of the role of biological sex after TBI has found many differences in the effects of injury as well as response to treatment in both animal models and humans (Cancelliere et al., 2016; Gupte et al., 2019; Rubin and Lipton, 2019). Thus, evaluation of whether these effects occur in female mice as well is a critical future direction.

Acknowledgements

We thank Eason Barclay for his help with analysis of SOM axotomized interneurons. We thank Susan A. Walker, Lynn Carol Davis, and Amanda Furman for their technical assistance in various aspects of this study.

References

Adams JH, et al. , 1991. Diffuse axonal injury in non-missile head injury. J. Neurol. Neurosurg. Psychiatry 54, 481–483. [PubMed: 1880506]

Antonoudiou P, et al. , 2020. Parvalbumin and somatostatin interneurons contribute to the generation of hippocampal gamma oscillations. J. Neurosci 40, 7668–7687. [PubMed: 32859716]

Avramescu S, et al. , 2009. Neocortical post-traumatic epileptogenesis is associated with loss of GABAergic neurons. J.Neurotrauma 26, 799–812. [PubMed: 19422294]

Babcock L, et al. , 2013. Predicting postconcussion syndrome after mild traumatic brain injury in children and adolescents who present to the emergency department. JAMA Pediatr 167, 156–161. [PubMed: 23247384]

Bazarian JJ, et al. , 2005. Mild traumatic brain injury in the United States, 1998–2000. Brain Inj 19, 85–91. [PubMed: 15841752]

Blumbergs PC, et al. , 1994. Staining of amyloid precursor protein to study axonal damage in mild head injury. Lancet 344, 1055–1056. [PubMed: 7523810]

Botterill JJ, et al. , 2017. Selective plasticity of hippocampal GABAergic interneuron populations following kindling of different brain regions. J. Comp. Neurol 525, 389–406. [PubMed: 27362579]

Cancelliere C, et al. , 2016. Is sex an indicator of prognosis after mild traumatic brain injury: a systematic analysis of the findings of the World Health Organization collaborating centre task force on mild traumatic brain injury and the international collaboration on mild traumatic brain injury prognosis. Arch. Phys. Med. Rehabil 97, S5–18. [PubMed: 25666784]

Cantu D, et al. , 2015. Traumatic brain injury increases cortical glutamate network activity by compromising GABAergic control. Cereb. Cortex 25, 2306–2320. [PubMed: 24610117]

Cardin JA, 2018. Inhibitory interneurons regulate temporal precision and correlations in cortical circuits. Trends Neurosci 41, 689–700. [PubMed: 30274604]

Cardin JA, et al. , 2009. Driving fast-spiking cells induces gamma rhythm and controls sensory responses. Nature 459, 663–667. [PubMed: 19396156]

Carron SF, et al. , 2016. Traumatic brain injury and neuronal functionality changes in sensory cortex. Front. Syst. Neurosci 10, 47. [PubMed: 27313514]

Carron SF, et al. , 2018. Immediate and medium-term changes in cortical and hippocampal inhibitory neuronal populations after diffuse TBI. Neuroscience 388, 152–170. [PubMed: 30036662]

Carron SF, et al. , 2020. Inhibitory neuronal changes following a mixed diffuse-focal model of traumatic brain injury. J. Comp. Neurol 528, 175–198. [PubMed: 31343072]

Celio MR, et al. , 1998. Perineuronal nets: past and present. Trends Neurosci 21, 510–515. [PubMed: 9881847]

Cho KK, et al. , 2015. Gamma rhythms link prefrontal interneuron dysfunction with cognitive inflexibility in Dlx5/6(+/−) mice. Neuron 85, 1332–1343. [PubMed: 25754826]

DeFelipe J, et al. , 2013. New insights into the classification and nomenclature of cortical GABAergic interneurons. Nat. Rev. Neurosci 14, 202–216. [PubMed: 23385869]

Del Pino I, et al. , 2013. Erbb4 deletion from fast-spiking interneurons causes schizophrenia-like phenotypes. Neuron 79, 1152–1168. [PubMed: 24050403]

Desai NS, et al. , 1999. Plasticity in the intrinsic excitability of cortical pyramidal neurons. Nat. Neurosci 2, 515–520. [PubMed: 10448215]

Evans MD, et al. , 2015. Rapid modulation of axon initial segment length influences repetitive spike firing. Cell Rep 13, 1233–1245. [PubMed: 26526995]

Fino E, Yuste R, 2011. Dense inhibitory connectivity in neocortex. Neuron 69, 1188–1203. [PubMed: 21435562]

Folweiler KA, et al. , 2020. Traumatic brain injury diminishes feedforward activation of parvalbumin-expressing interneurons in the dentate gyrus. eNeuro 7.

Frankowski JC, et al. , 2019. Selective vulnerability of hippocampal interneurons to graded traumatic brain injury. Neurobiol. Dis 129, 208–216. [PubMed: 30031783]

Frankowski JC, et al. , 2021. Traumatic brain injury to primary visual cortex produces long-lasting circuit dysfunction. Commun. Biol 4, 1297. [PubMed: 34789835]

Fries P, et al. , 2007. The gamma cycle. Trends Neurosci 30, 309–316. [PubMed: 17555828]

George AL, Jacobs KM, 2011. Altered intrinsic properties of neuronal subtypes in malformed epileptogenic cortex. Brain Res 1374, 116–128. [PubMed: 21167139]

Gibson JR, et al. , 1999. Two networks of electrically coupled inhibitory neurons in neocortex. Nature 402, 75–79. [PubMed: 10573419]

Gouwens NW, et al. , 2020. Integrated morphoelectric and transcriptomic classification of cortical GABAergic cells. Cell 183, 935–953.e19. [PubMed: 33186530]

Greer JE, et al. , 2011. Diffuse traumatic axonal injury in the mouse induces atrophy, c-Jun activation, and axonal outgrowth in the axotomized neuronal population. J. Neurosci 31, 5089–5105. [PubMed: 21451046]

Greer JE, et al. , 2012. Electrophysiological abnormalities in both axotomized and nonaxotomized pyramidal neurons following mild traumatic brain injury. J. Neurosci 32, 6682–6687. [PubMed: 22573690]

Greer JE, et al. , 2013. Mild traumatic brain injury in the mouse induces axotomy primarily within the axon initial segment. Acta Neuropathol 126, 59–74. [PubMed: 23595276]

Griffiths BB, et al. , 2019. Pre-treatment with microRNA-181a antagomir prevents loss of parvalbumin expression and preserves novel object recognition following mild traumatic brain injury. NeuroMolecular Med 21, 170–181. [PubMed: 30900118]

Gu F, et al. , 2017. Structural alterations in fast-spiking GABAergic interneurons in a model of posttraumatic neocortical epileptogenesis. Neurobiol. Dis 108, 100–114. [PubMed: 28823934]

Gupta A, et al. , 2012. Decrease in tonic inhibition contributes to increase in dentate semilunar granule cell excitability after brain injury. J. Neurosci 32, 2523–2537. [PubMed: 22396425]

Gupte R, et al. , 2019. Sex differences in traumatic brain injury: what we know and what we should know. J. Neurotrauma 36, 3063–3091. [PubMed: 30794028]

Hakim R, et al. , 2018. A neural circuit for gamma-band coherence across the retinotopic map in mouse visual cortex. Elife 7.

Hameed MQ, et al. , 2019. Ceftriaxone treatment preserves cortical inhibitory interneuron function via transient salvage of GLT-1 in a rat traumatic brain injury model. Cereb. Cortex 29, 4506–4518. [PubMed: 30590449]

Hånell A, et al. , 2015a. Increased network excitability due to altered synaptic inputs to neocortical layer V intact and axotomized pyramidal neurons after mild traumatic brain injury. J. Neurotrauma 32, 1590–1598. [PubMed: 25789412]

Hånell A, et al. , 2015b. Traumatic brain injury-induced axonal phenotypes react differently to treatment. Acta Neuropathol 129, 317–332. [PubMed: 25528329]

Hilscher MM, et al. , 2017. Chrna2-martinotti cells synchronize layer 5 type a pyramidal cells via rebound excitation. PLoS Biol 15, e2001392. [PubMed: 28182735]

Hsieh TH, et al. , 2017. Trajectory of parvalbumin cell impairment and loss of cortical inhibition in traumatic brain injury. Cereb. Cortex 27, 5509–5524. [PubMed: 27909008]

Hu H, et al. , 2014. Interneurons. Fast-spiking, parvalbumin^{+} GABAergic interneurons: from cellular design to microcircuit function. Science 345, 1255263. [PubMed: 25082707]

Hunt RF, et al. , 2011. Synaptic reorganization of inhibitory hilar interneuron circuitry after traumatic brain injury in mice. J. Neurosci 31, 6880–6890. [PubMed: 21543618]

Huusko N, et al. , 2015. Loss of hippocampal interneurons and epileptogenesis: a comparison of two animal models of acquired epilepsy. Brain Struct. Funct 220, 153–191. [PubMed: 24096381]

Jiang X, et al. , 2015. Principles of connectivity among morphologically defined cell types in adult neocortex. Science 350, aac9462.

Jonas P, et al. , 2004. Interneuron Diversity series: Fast in, fast out–temporal and spatial signal processing in hippocampal interneurons. Trends Neurosci 27, 30–40. [PubMed: 14698608]

Kawata M, et al. , 2017. Ablation of neuropsin-neuregulin 1 signaling imbalances ErbB4 inhibitory networks and disrupts hippocampal gamma oscillation. Transl. Psychiatry 7, e1052. [PubMed: 28267150]

Kinnunen KM, et al. , 2011. White matter damage and cognitive impairment after traumatic brain injury. Brain 134, 449–463. [PubMed: 21193486]

Knott GW, et al. , 2002. Formation of dendritic spines with GABAergic synapses induced by whisker stimulation in adult mice. Neuron 34, 265–273. [PubMed: 11970868]

Kuruba R, et al. , 2011. Differential susceptibility of interneurons expressing neuropeptide Y or parvalbumin in the aged hippocampus to acute seizure activity. PLoS One 6, e24493. [PubMed: 21915341]

Lowenstein DH, et al. , 1992. Selective vulnerability of dentate hilar neurons following traumatic brain injury: a potential mechanistic link between head trauma and disorders of the hippocampus. J. Neurosci 12, 4846–4853. [PubMed: 1464770]

MacMullin P, et al. , 2020. Increase in seizure susceptibility after repetitive concussion results from oxidative stress, parvalbumin-positive interneuron dysfunction and biphasic increases in glutamate/GABA ratio. Cereb. Cortex 30, 6108–6120. [PubMed: 32676666]

Markram H, et al. , 2004. Interneurons of the neocortical inhibitory system. Nat. Rev. Neurosci 5, 793–807. [PubMed: 15378039]

Marx M, et al. , 2013. Differential vulnerability of interneurons in the epileptic hippocampus. Front. Cell. Neurosci 7, 167. [PubMed: 24098270]

McMahon P, et al. , 2014. Symptomatology and functional outcome in mild traumatic brain injury: results from the prospective TRACK-TBI study. J. Neurotrauma 31, 26–33. [PubMed: 23952719]

Nichols J, et al. , 2018. Parvalbumin fast-spiking interneurons are selectively altered by paediatric traumatic brain injury. J. Physiol 596, 1277–1293. [PubMed: 29333742]

Pfeffer CK, et al. , 2013. Inhibition of inhibition in visual cortex: the logic of connections between molecularly distinct interneurons. Nat. Neurosci 16, 1068–1076. [PubMed: 23817549]

Pizzo R, et al. , 2016. Lack of Cdkl5 disrupts the organization of excitatory and inhibitory synapses and parvalbumin interneurons in the primary visual cortex. Front. Cell. Neurosci 10, 261. [PubMed: 27965538]

Pouille F, Scanziani M, 2001. Enforcement of temporal fidelity in pyramidal cells by somatic feed-forward inhibition. Science 293, 1159–1163. [PubMed: 11498596]

Povlishock JT, Becker DP, Cheng CL, Vaughan GW, 1983. Axonal change in minor head injury. J. Neuropathol. Exp. Neurol 42, 225–242. [PubMed: 6188807]

Povlishock JT, Christman CW, 1995. The pathobiology of traumatically induced axonal injury in animals and humans: a review of current thoughts. J. Neurotrauma 12 (4), 555–564. [PubMed: 8683606]

Rubin TG, Lipton ML, 2019. Sex differences in animal models of traumatic brain injury. J. Exp. Neurosci 13, 1179069519844020. [PubMed: 31205421]

Rudy B, et al. , 2011. Three groups of interneurons account for nearly 100% of neocortical GABAergic neurons. Dev. Neurobiol 71, 45–61. [PubMed: 21154909]

Santhakumar V, et al. , 2000. Granule cell hyperexcitability in the early post-traumatic rat dentate gyrus: the ‘irritable mossy cell’ hypothesis. J. Physiol 524 (Pt 1), 117–134. [PubMed: 10747187]

Santhakumar V, et al. , 2001. Long-term hyperexcitability in the hippocampus after experimental head trauma. Ann.Neurol 50, 708–717. [PubMed: 11761468]

Shultz SR, et al. , 2017. The potential for animal models to provide insight into mild traumatic brain injury: translational challenges and strategies. Neurosci. Biobehav. Rev 76, 396–414. [PubMed: 27659125]

Silberberg G, Markram H, 2007. Disynaptic inhibition between neocortical pyramidal cells mediated by Martinotti cells. Neuron 53, 735–746. [PubMed: 17329212]

Sloviter RS, 1987. Decreased hippocampal inhibition and a selective loss of interneurons in experimental epilepsy. Science 235, 73–76. [PubMed: 2879352]

Sloviter RS, 1989. Calcium-binding protein (calbindin-D28k) and parvalbumin immunocytochemistry: localization in the rat hippocampus with specific reference to the selective vulnerability of hippocampal neurons to seizure activity. J. Comp. Neurol 280, 183–196. [PubMed: 2925892]

Sloviter RS, et al. , 1991. Calcium-binding protein (calbindin-D28K) and parvalbumin immunocytochemistry in the normal and epileptic human hippocampus. J. Comp. Neurol 308, 381–396. [PubMed: 1865007]

Smith DH, Hicks R, Povlishock JT, 2013. Therapy development for diffuse axonal injury. J. Neurotrauma 30 (5), 307–323. [PubMed: 23252624]

Sohal VS, et al. , 2009. Parvalbumin neurons and gamma rhythms enhance cortical circuit performance. Nature 459, 698–702. [PubMed: 19396159]

Swanwick CC, et al. , 2006. Activity-dependent scaling of GABAergic synapse strength is regulated by brain-derived neurotrophic factor. Mol. Cell. Neurosci 31, 481–492. [PubMed: 16330218]

Toth Z, et al. , 1997. Instantaneous perturbation of dentate interneuronal networks by a pressure wave-transient delivered to the neocortex. J.Neurosci 17, 8106–8117. [PubMed: 9334386]

Tucker LB, et al. , 2019. Sex differences in cued fear responses and parvalbumin cell density in the hippocampus following repetitive concussive brain injuries in C57BL/6J mice. PLoS One 14, e0222153. [PubMed: 31487322]

Turrigiano GG, Nelson SB, 2004. Homeostatic plasticity in the developing nervous system. Nat. Rev. Neurosci 5, 97–107. [PubMed: 14735113]

Urban-Ciecko J, et al. , 2015. Neocortical somatostatin neurons reversibly silence excitatory transmission via GABAb receptors. Curr. Biol 25, 722–731. [PubMed: 25728691]

van Eijck MM, et al. , 2018. Diffuse axonal injury after traumatic brain injury is a prognostic factor for functional outcome: a systematic review and meta-analysis. Brain Inj 32, 395–402. [PubMed: 29381396]

Vascak M, et al. , 2017. Mild traumatic brain injury evokes pyramidal neuron axon initial segment plasticity and diffuse presynaptic inhibitory terminal loss. Front. Cell. Neurosci 11, 157. [PubMed: 28634442]

Vascak M, et al. , 2018. Mild traumatic brain injury induces structural and functional disconnection of local neocortical inhibitory networks via parvalbumin interneuron diffuse axonal injury. Cereb. Cortex 28, 1625–1644. [PubMed: 28334184]

Veit J, et al. , 2017. Cortical gamma band synchronization through somatostatin interneurons. Nat. Neurosci 20, 951–959. [PubMed: 28481348]

Vogt D, et al. , 2015. The parvalbumin/somatostatin ratio is increased in Pten mutant mice and by human PTEN ASD alleles. Cell Rep 11, 944–956. [PubMed: 25937288]

Wiley CA, et al. , 2016. Ultrastructure of diaschisis lesions after traumatic brain injury. J. Neurotrauma 33, 1866–1882. [PubMed: 26914973]

Wingert JC, Sorg BA, 2021. Impact of perineuronal nets on electrophysiology of parvalbumin interneurons, principal neurons, and brain oscillations: a review. Front. Synaptic. Neurosci 13, 673210. [PubMed: 34040511]

Yavorska I, Wehr M, 2016. Somatostatin-expressing inhibitory interneurons in cortical circuits. Front. Neural. Circuits 10, 76. [PubMed: 27746722]

Yuh EL, et al. , 2013. Magnetic resonance imaging improves 3-month outcome prediction in mild traumatic brain injury. Ann. Neurol 73, 224–235. [PubMed: 23224915]

Zhang BL, et al. , 2018. Cognitive impairment after traumatic brain injury is associated with reduced long-term depression of excitatory postsynaptic potential in the rat hippocampal dentate gyrus. Neural Regen. Res 13, 1753–1758. [PubMed: 30136690]

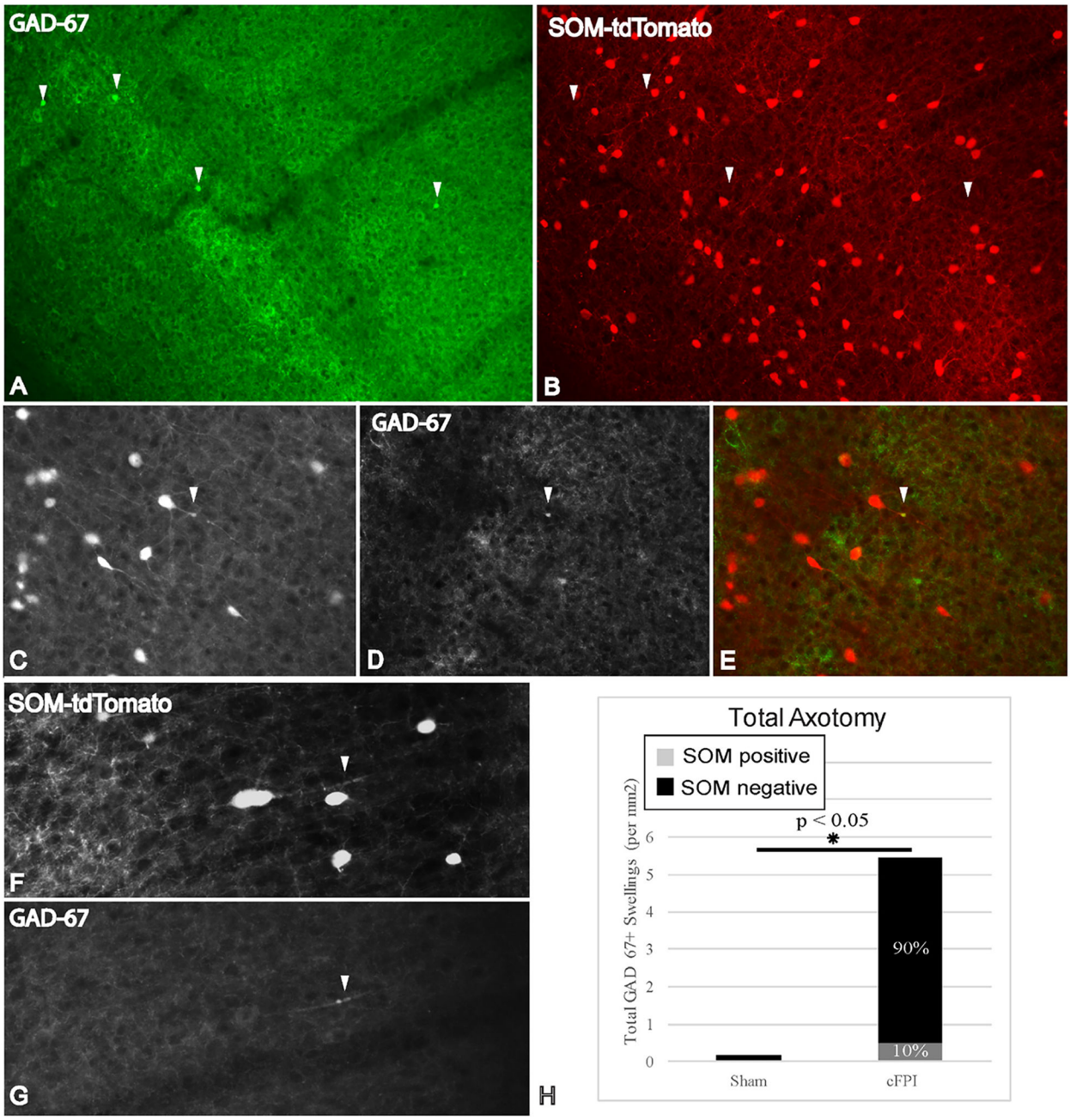

Fig. 1.

Limited SOM axotomy following mTBI known to create TAI. Within 3 h post-injury GAD67+ swellings were readily identified throughout layers 2–6 of somatosensory cortex. The vast majority of GAD67+ swellings (A) did not demonstrate expression of tdTomato driven by somatostatin (B). These GAD67+/SS− swellings were sometimes found isolated from the cell body of origin but more often localized to the perisomatic domain. Isolated GAD67+/SS+ swellings were occasionally noted, also occurring either isolated or perisomatically (C-G). Quantitative analysis demonstrated a significant increase in both GAD67+/SS− (*t*-test, $p = 0.021$) and GAD67+/SS+ (t-test, $p = 0.021$) swellings compared to

sham (H). Importantly, GAD67+/SS+ swellings constituted only 10% of the total GAD67+ swellings.

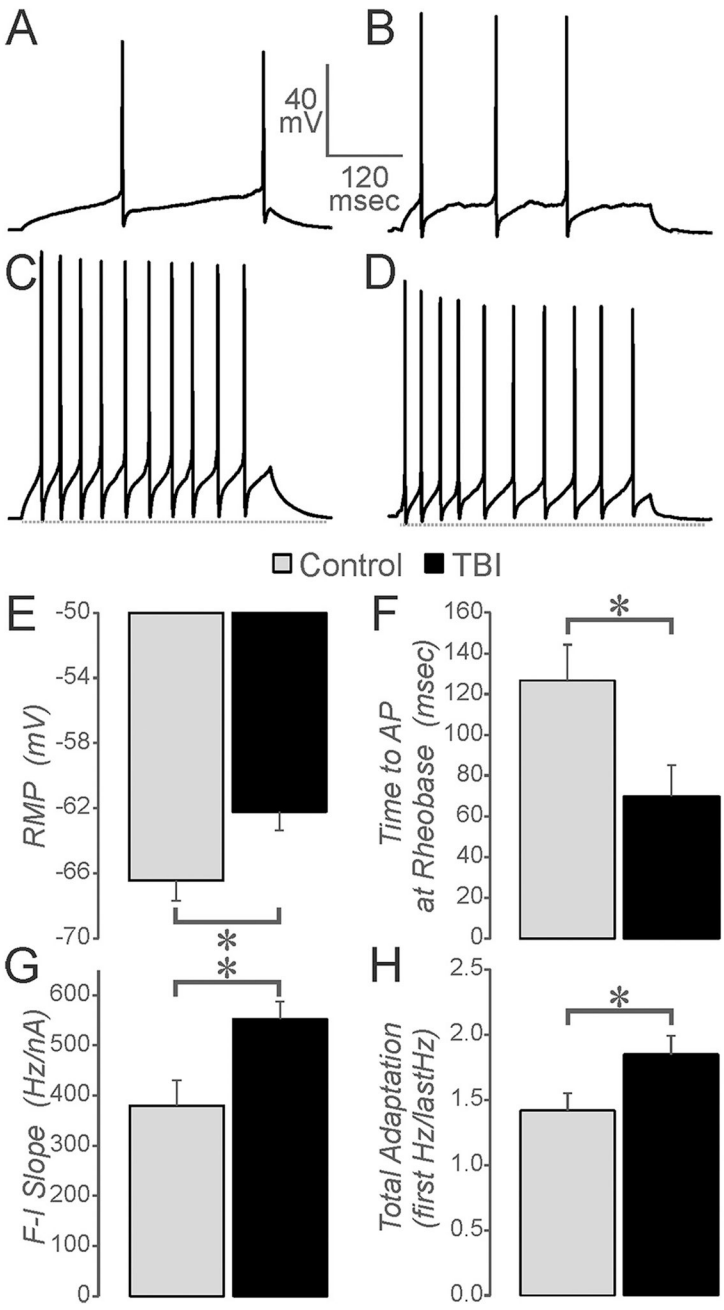

Fig. 2.

Intrinsic and membrane properties of SOM neurons are altered after mTBI. A & B. Action potential firing examples at rheobase for control (A) and mTBI (B). C & D. Examples of adaptation that arises during a train of 10 action potentials per 400 msec sweep, for control (C) and TBI (D). Dashed line demonstrates the more hyperpolarized level for the first compared to the last afterhyperpolarization in the train for both control and TBI cells. E. Resting membrane potential (RMP) was significantly more depolarized in the TBI group. F. The time to the first action potential was significantly shorter in the TBI group. G. The slope of the plot of sweep action potential frequency versus injected current was

significantly larger in the TBI group. The total adaptation (frequency of first two action potentials/frequency of last two action potentials) for sweeps with 8–10 action potentials was greater in the TBI group. In all cases * = t-test, $p < 0.05$, for 17 control cells from 6 mice and 24 TBI cells from 4 mice.

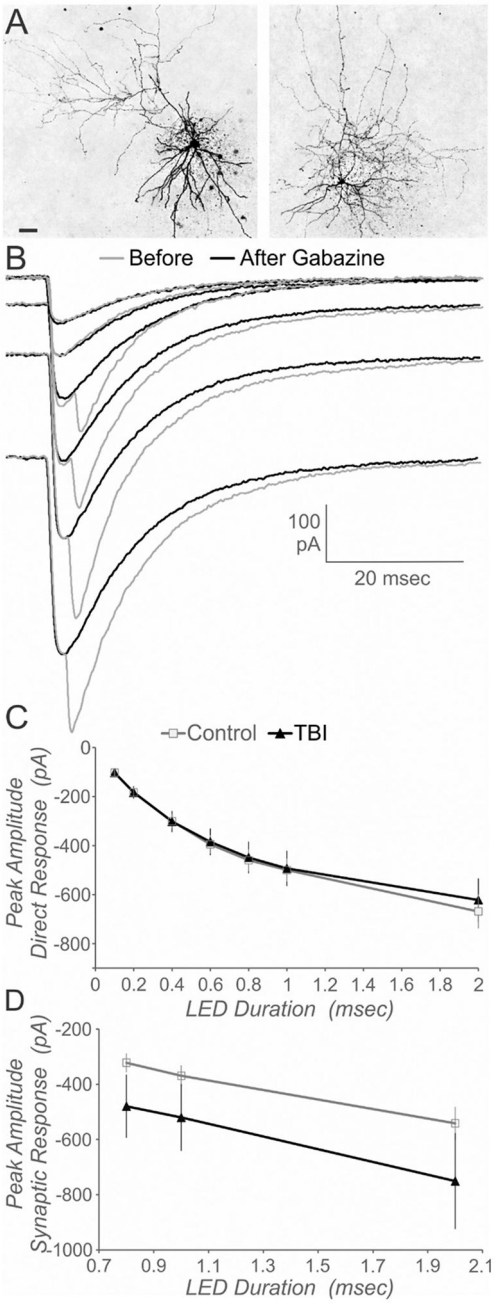

Fig. 3.

Responses recorded in fluorescing SOM interneurons in response to activation of ChR2 within SOM interneurons. A. Photomicrographs of example filled neurons. Scale bar is 40 μm. B. Example responses recorded in SOM neurons to ChR2 activation. At durations of 0.6 msec and above, two peaks are apparent (gray lines). Bath application of gabazine abolished the second peak, indicating this component represents a SOM to SOM synaptic response. The remaining peak (black lines) is due to direct ChR2 activation of the SOM interneuron being recorded. C. The direct activation of SOM via ChR2 was not different in TBI compared to control cells. Repeated Measures ANOVA, $p > 0.05$, $n = 13$ SOM

interneurons from 2 control mice and 12 SOM interneurons from 3 TBI mice. D. The synaptic response was observed in 11 of 13 control and 9 of 12 mTBI SOM interneurons. The peak of the synaptic response was also not significantly different between subject groups. Repeated Measures ANOVA, $P > 0.05$.

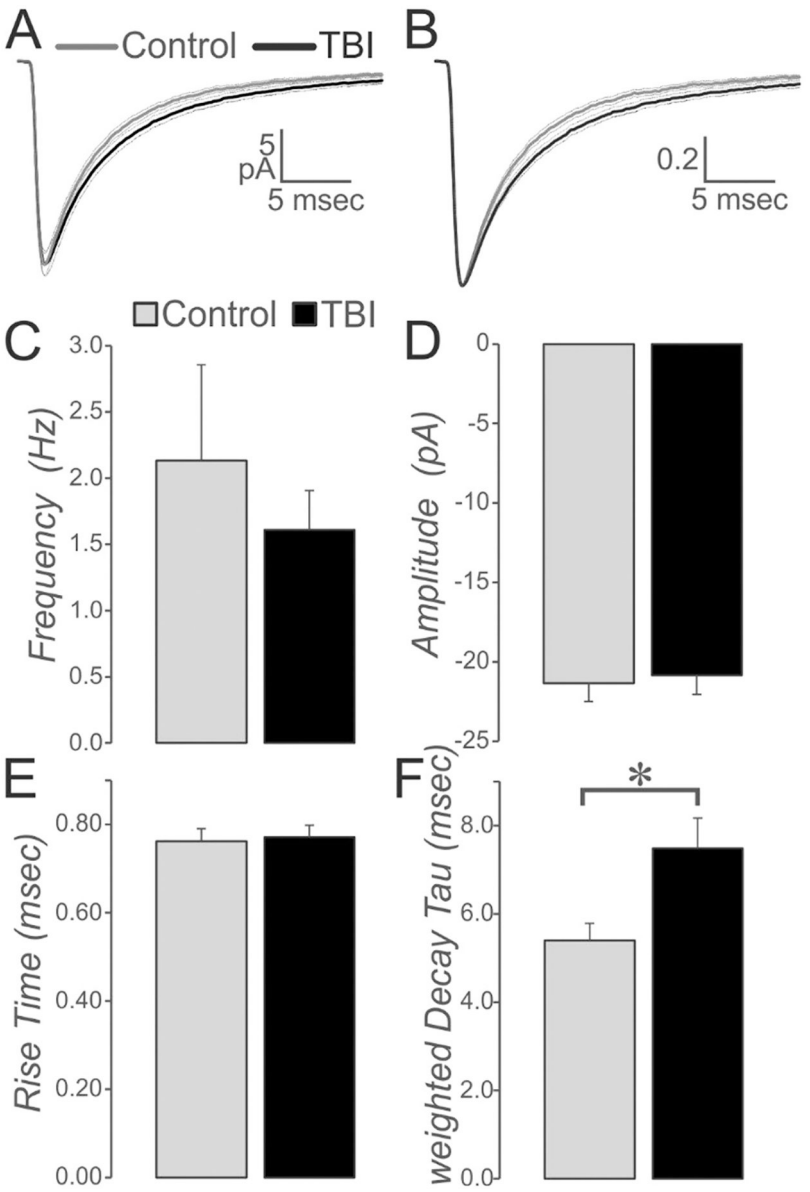

Fig. 4.

Spontaneous inhibitory currents recorded in SOM interneurons. A. All Type I events (events with no overlap with other events) were averaged within each neuron and then averaged across neurons for each subject group (sham in black, TBI in gray), with SEM shown in dashed lines around mean. B. Same as in A, but here the average was normalized to the peak for better visualization of differences in decay timing. There was no significant difference in sIPSC frequency (C), amplitude (D), or rise time (E). The weighted Decay Tau was significantly slower in the TBI group. For these measures a t-test was used, with * = $p < 0.05$, for 15 neurons from 2 control mice and 26 neurons from 3 TBI mice.

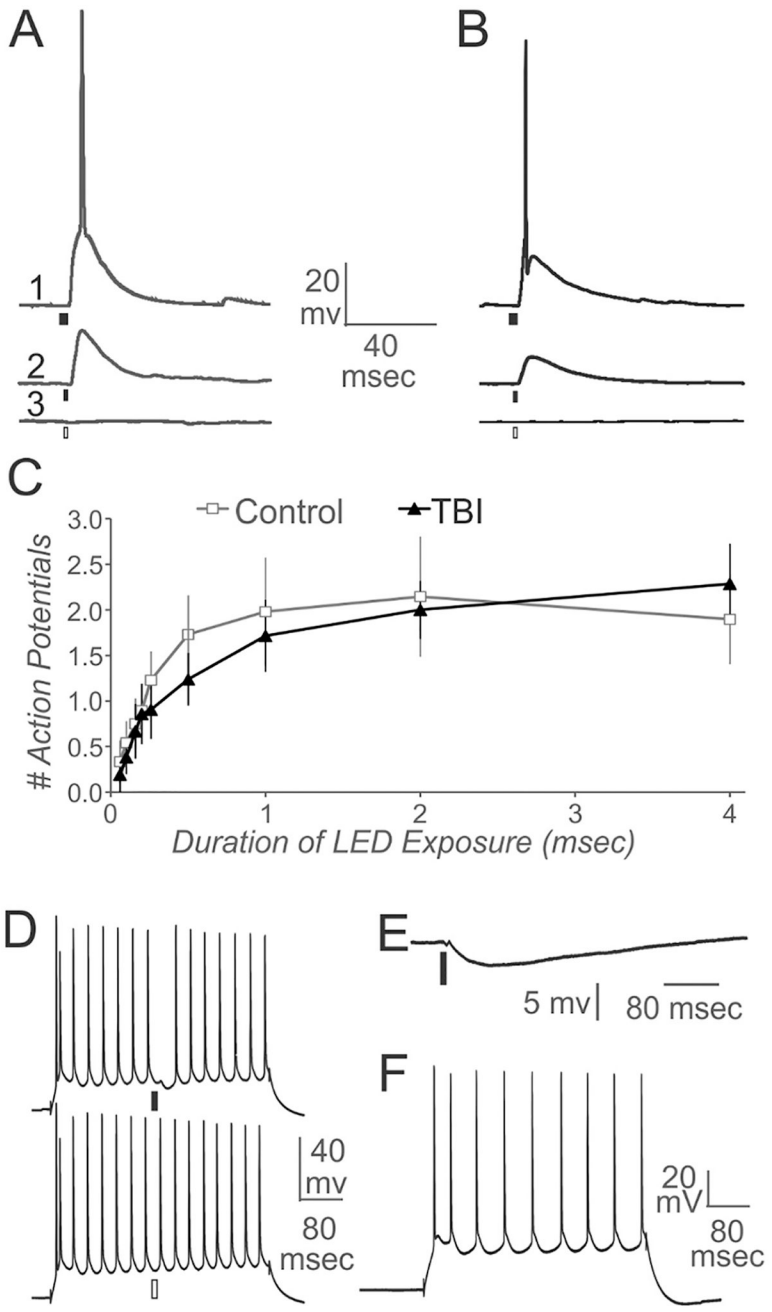

Fig. 5.

Effects of activating ChR2 expressed in SOM interneurons. A, B. Examples of responses of SOM interneurons from control (A) and mTBI (B) animals after long (1) or short (2) pulses of blue light or yellow light (3). C. The number of action potentials produced after varying durations of blue light pulses was similar in control and mTBI groups (repeated measures ANOVA, $p > 0.05$, $n = 9$ SOM interneurons from 6 control mice and 7 SOM interneurons from 3 TBI mice). D–F. Recordings from pyramidal neurons during blue light pulses. D. A 400 msec depolarizing pulse produced action potentials within the pyramidal neuron. Yellow light (bottom) had no effect on this action potential train, while blue light (top) aborted the

next action potential. E. Blue light pulse given at resting membrane potential in a pyramidal neuron produced an IPSP. F. This non-fluorescing neuron demonstrated an action potential firing pattern typical of pyramidal neurons, in which the first AHP was shorter and more depolarized than the last AHP in the train.

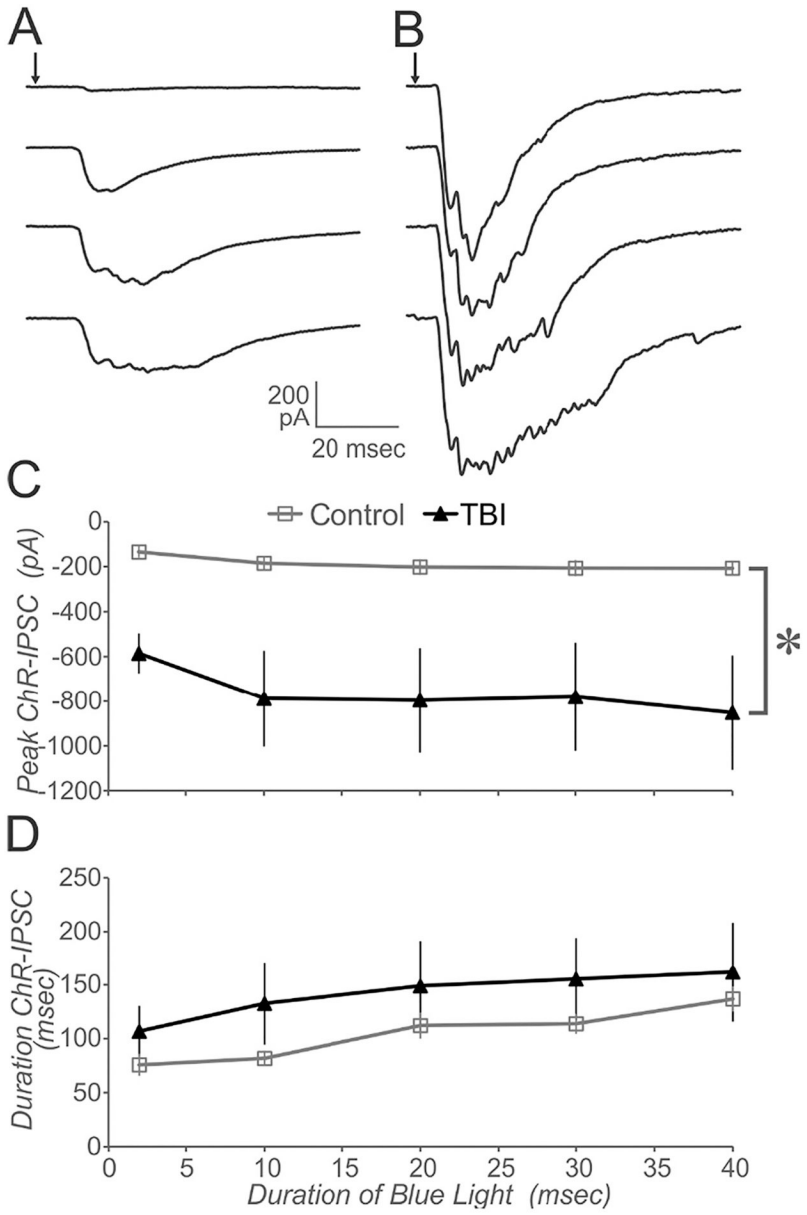

Fig. 6.

ChR2-IPSCs recorded within pyramidal neurons. A, B. Examples of responses to increasing blue light durations applied through the objective above the recorded neuron (2, 10, 30, and 40 msec) in control (A) and mTBI (B). Each waveform is the average of 3 light presentations. Arrow indicates timing of light onset. C. Peak ChR2-IPSC for control (squares, gray line) and mTBI (triangles, black line) across different durations of blue light stimulation. D. Duration of the evoked ChR2-IPSC for same responses as in C. For C and D, repeated measures ANOVA was performed, $n = 14$ pyramidal neurons from 5 control mice and 11 pyramidal neurons from 4 TBI mice, * = significantly different, $p < 0.05$.

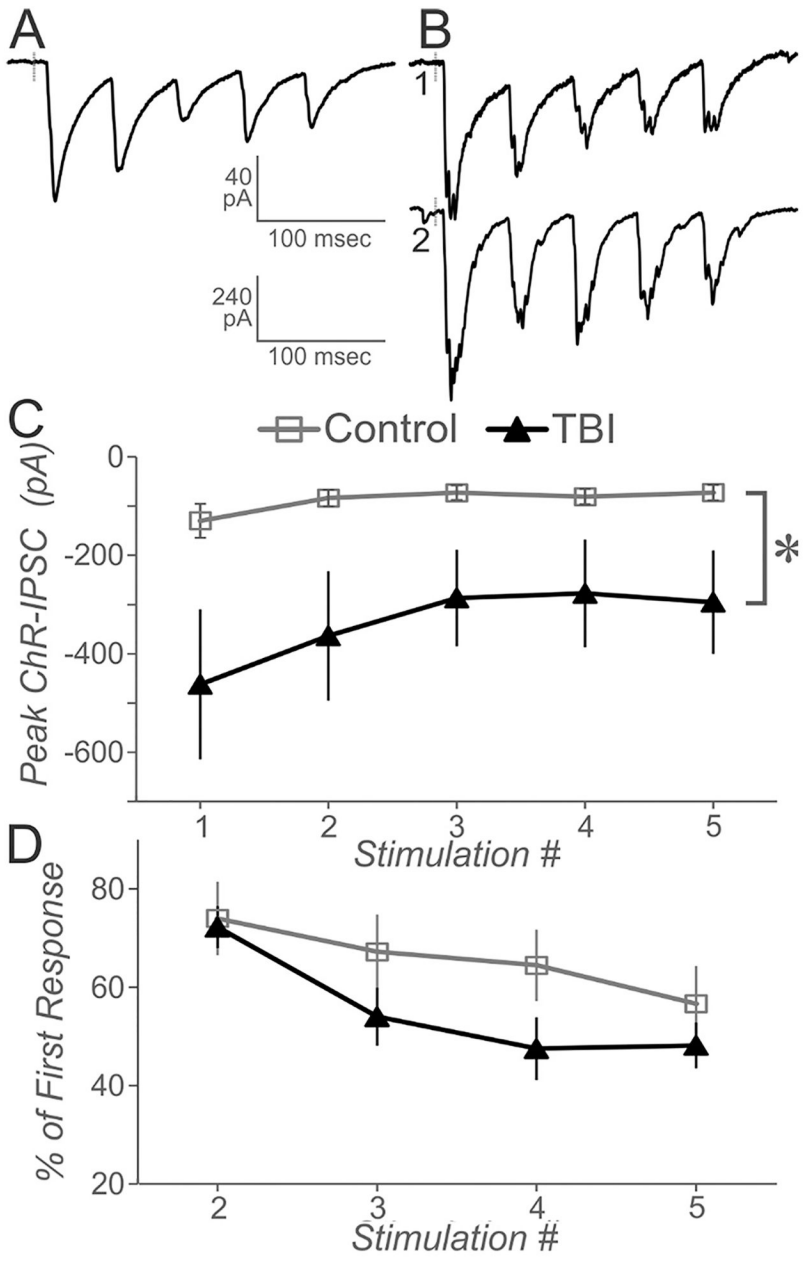

Fig. 7.

Repetitive ChR2-IPSCs evoked in pyramidal neurons with 2 msec long blue light pulses given at 20 Hz. A, B Five sweep averages show typical responses for control (A) and mTBI (B). Upper scale bar for A and B_1. Lower scale bar for B_2. Starting amplitude for the mTBI was variable, but degree of depression was similar in both cases. C. Peak amplitude of the ChR2-IPSC for control (squares, gray line) and mTBI (triangles, black line), for 13 pyramidal neurons from 5 control mice and 11 pyramidal neurons from 4 TBI mice. D. Synaptic depression shown as the peak response for stimuli 2–5 divided by peak response for stimuli 1. Control and mTBI were not significantly different in the degree of depression (2-way repeated measures ANOVA, $p > 0.05$).

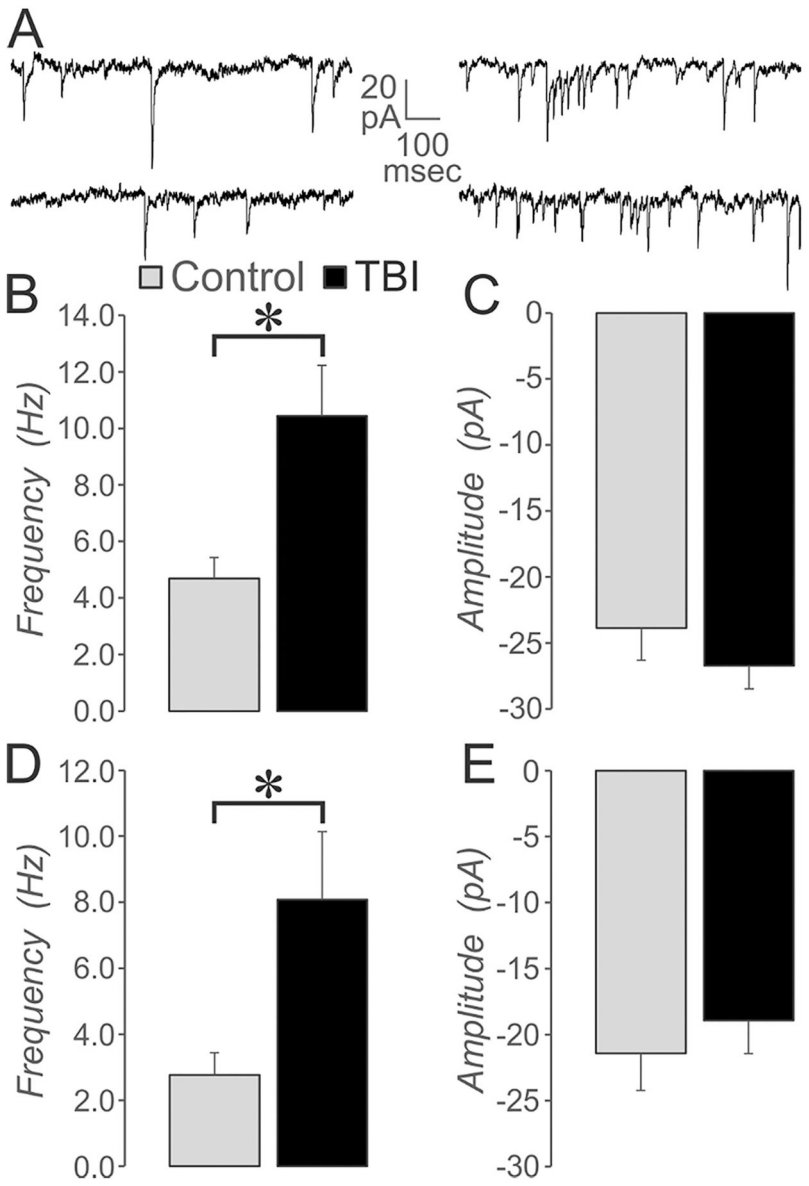

Fig. 8.

Spontaneous IPSCs recorded in pyramidal neurons. A. Examples of sIPSCs (upper row) and mIPSCs (lower row) recorded in pyramidal neurons from control (left panel) and mTBI (right panel). The frequency of both sIPSCs (B) and mIPSCs (D) was significantly higher in pyramidal neurons of mTBI compared to control cortex. * = $p < 0.05$, *t*-tests, $n = 26$ neurons from 10 control mice and 23 neurons from 9 TBI mice for sIPSCs and 13 neurons from 5 control mice and 9 neurons from 3 TBI mice for mIPSCs. The amplitude of both sIPSCs and mIPSCs was not significantly different between control and mTBI.

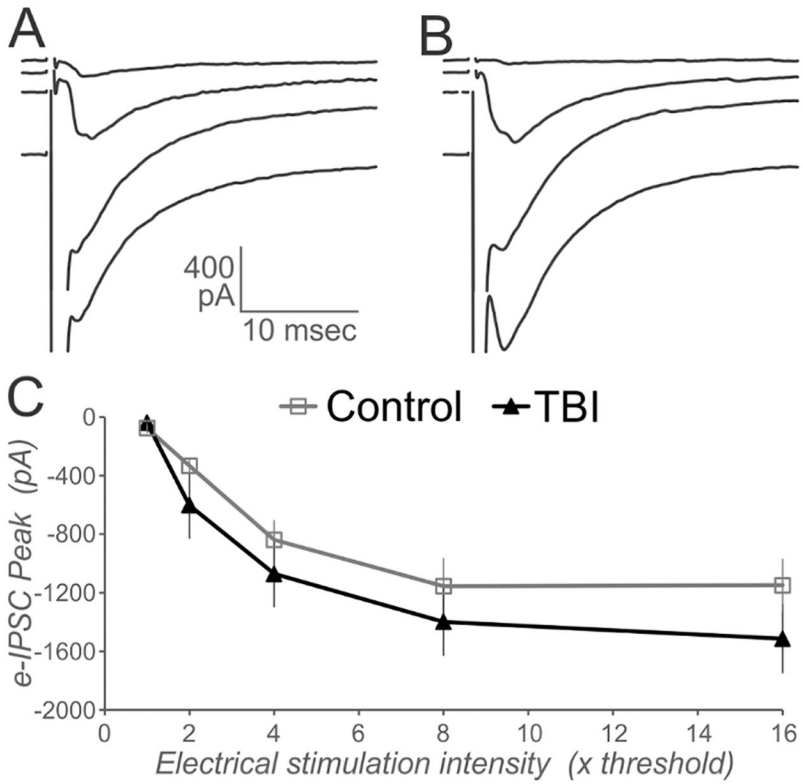

Fig. 9.

Electrically-evoked IPSC recorded in pyramidal neurons. Threshold stimulation produced an IPSC on ~50% of trials. Stimulation intensity was then successively increased by doubling the stimulation time. A, B. Shown are typical examples from control (A) and mTBI (B), which are averages of 3 stimulus presentations for 1× – 8×, after which the responses plateaued. C. Peak amplitude of the e-IPSC was not significantly different between control and mTBI groups, $n = 24$ pyramidal neurons from 4 control mice and 15 pyramidal neurons from 4 TBI mice, 2-way repeated measures ANOVA, $p > 0.05$.

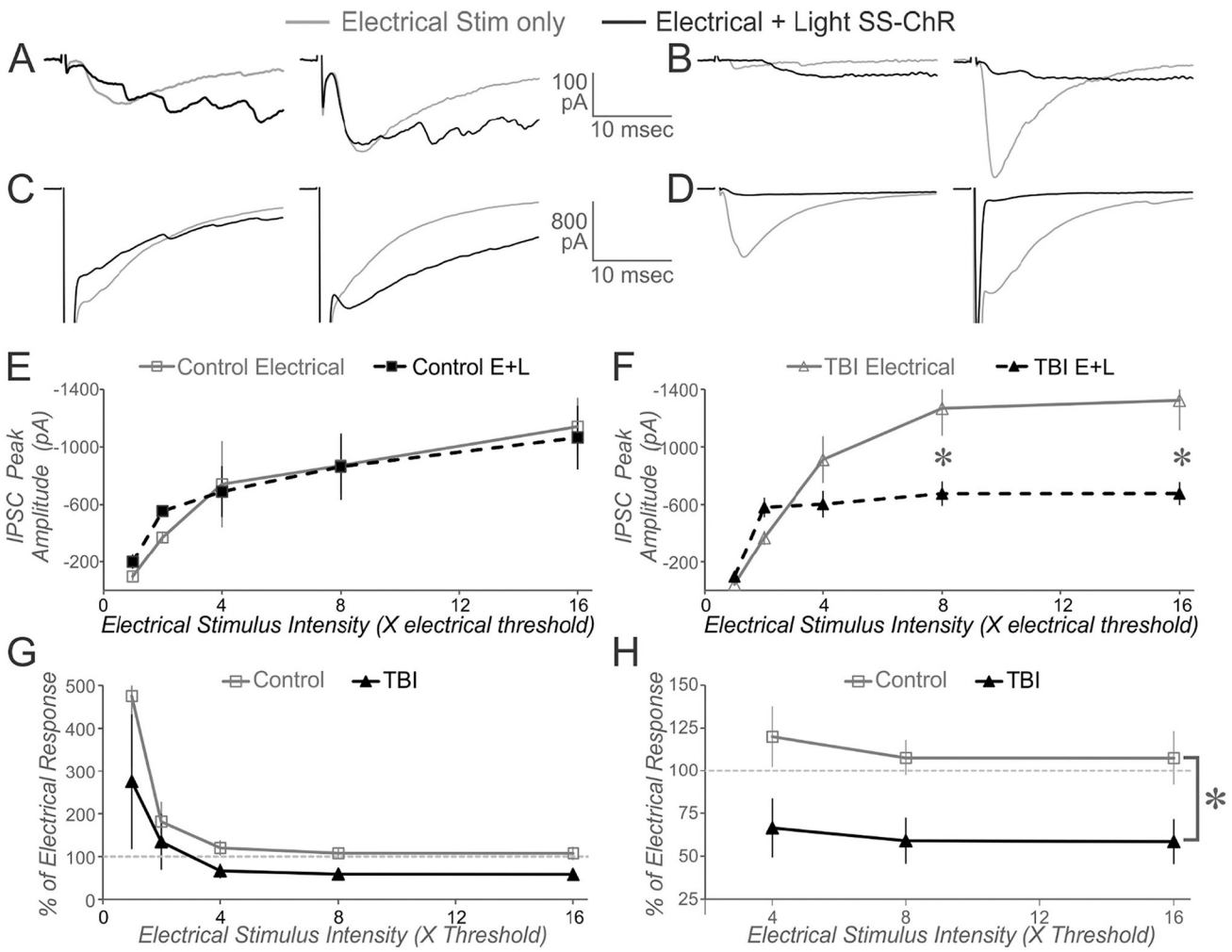

Fig. 10.

The effect of adding SOM-ChR2 activation to the electrically evoked IPSC. The electrical stimulation was applied as shown in Fig. 9 (gray lines in A-D). In subsequent stimulus applications, blue light was applied immediately after the electrical stimulus for 70 msec (black lines in A-D). Shown are responses to electrical stimulation intensities of 1× and 2× for control (A) and mTBI (B), and for 4× and 8× for control (C) and mTBI (D). E. Control responses. Shown are the peak amplitude for electrical stimulation alone (gray solid line) and for electrical plus light to activate the ChR2 in SOM interneurons (E + L, black dashed line). These were not significantly different, 2-way repeated measures ANOVA, n = 14 paired responses from the same cells. F. Same as E, except for mTBI cortex. A 2-way repeated measures ANOVA showed a significant interaction between condition and stimulus intensity, $n = 11$. Posthoc analysis showed that the two highest electrical intensities showed a difference between electrical only and electrical + light. G. The peak response in the electrical plus light condition was divided by the peak response in the electrical only condition to generate a percent change for each recorded neuron by stimulus intensity. H. Expansion of the highest 3 electrical stimulating intensities shown in G. A 2-way repeated measures ANOVA showed a significant difference between control and TBI groups, n = 14

pyramidal neurons from 8 control mice and 11 pyramidal neurons from 4 TBI mice, * = $p < 0.05$.

Table 1

Characteristics of SOM interneurons. No significant differences. $N = 17$ control and 24 TBI interneurons.

	AP Threshold (mV)	Rin (MΩ)	Rheobase (pA)
Control	−49.5 ± 0.8	166.3 ± 18.9	54.1 ± 12.2
TBI	−51.0 ± 0.6	179.3 ± 15.3	38.8 ± 5.6